Spin-Dependent Low-Energy $^4He^+$ Ion Scattering from Nonmagnetic Surfaces

T. T. Suzuki,* Y. Yamauchi, and S. Hishita

National Institute for Materials Science, 1-1 Namiki, Tsukuba, Ibaraki 305-0044, Japan

(Received 25 July 2011; published 18 October 2011)

We investigated electron-spin-polarized $^4He^+$ ion scattering on various nonmagnetic surfaces at kinetic energies below 2 keV. It was observed that the scattered He^+ ion yield depends on the He^+ ion spin. We interpret this spin-dependent scattering in terms of the spin-orbit coupling that acts transiently on the $He^+ 1s$ electron spin in the He^+-target binary collision. This interpretation qualitatively explains the relationship between the spin-dependent scattering and the scattering geometry, incident velocity, and magnetic field arrangement. This is the first study to report spin-orbit coupling caused by projectile electron spin in ion scattering.

DOI: 10.1103/PhysRevLett.107.176101 PACS numbers: 68.49.Sf, 34.80.Nz, 79.20.Rf

Low-energy ion beams, typically He^+ ion beams with kinetic energies of a few keV, have been widely used to analyze the outermost surfaces of solids [1,2]. The ionization energy of helium is so large (24.6 eV) that He^+ ions are neutralized on surfaces typically via the interatomic Auger process (Auger neutralization) with quite high probability [1,3,4]. In Auger neutralization, the spin of a surface electron filling the $He^+ 1s$ hole should be opposite to that of the $He^+ 1s$ electron because of the Pauli exclusion principle [5]. Thus, the survival probability P_S of the projectile He^+ ions on electron-spin-polarized surfaces, i.e., magnetic surfaces, varies with the electron spins of the projectiles [6,7]. The spin dependence of P_S is estimated from the scattered He^+ ion yield I ($\propto P_S\sigma$, where σ is a scattering cross section). If σ is spin independent, the surface spin polarization can be analyzed by using the spin dependence of I, that is, the spin asymmetry (spin-polarized ion scattering spectroscopy, SP-ISS [8]). The spin independence of σ has been assumed for projectiles with kinetic energies of several keV or less. [1]. In addition, a similar analysis using an electron-spin-polarized metastable helium-4 atom 2^3S_1 (He^*) beam with thermal kinetic energy has been widely employed in surface spin polarization analyses (spin-polarized metastable deexcitation spectroscopy, SP-MDS [9]). These techniques have attracted much attention because of their unique ability to selectively analyze the outermost surface magnetism, which can greatly differ from that of the bulk [10–14].

If the spin asymmetry is purely due to the survival probability of the projectile He^+ ions, it should not appear on nonmagnetic surfaces because no electron spin polarization is present. Previous SP-ISS and SP-MDS studies have consistently observed no spin asymmetry on nonmagnetic surfaces [9,15–18]. This supports the abovementioned assumption of spin-independent scattering cross sections in low-energy ion scattering (LEIS).

In nuclear physics, the spin-dependent cross section is well known to arise from spin-orbit coupling (SOC) in high-energy ion scattering [19]. It is intuitively interpreted as the effect on the projectile spin $\mathbf{S}$ of the magnetic field $\mathbf{H}$ induced by the projectile angular motion around the target nucleus during the projectile-target binary collision. The target nucleus can be considered to rotate around the projectile in the binary collision (Biot-Savart law); the SOC potential U_{SOC} in the collision between a projectile of mass M_1 and a target of atomic number Z_2 has the following form:

$$U_{\mathrm{SOC}} = \mathbf{H}\cdot\mathbf{S} \propto (Z_2/|\mathbf{r}|^3)(\mathbf{r}\times M_1\mathbf{v})\cdot\mathbf{S}, \qquad (1)$$

where $\mathbf{v}$ is the velocity of the projectile and $\mathbf{r}$ is the position of the target nucleus as seen from the projectile. An increase in the collisional energy enhances U_{SOC} because v increases and r decreases. In fact, SOC in ion scattering has been observed only in high-energy ion scattering using nuclear-spin-polarized projectiles with incident energies of more than 1 MeV [20–22]. On the other hand, SOC in LEIS has been traditionally treated as a negligible effect; the scattering has been interpreted in terms of only a central force potential, which is a screened Coulomb potential [1]. To the best of our knowledge, no study has reported SOC in LEIS.

In this Letter, we report that low-energy He^+ ion scattering depends on the $He^+ 1s$ electron spins, even on nonmagnetic surfaces. A detailed analysis of this spin-dependent scattering reveals the role of SOC in the He^+ ion-target-atom binary collision. Thus, this Letter for the first time demonstrates the effect of SOC on the scattering cross section in LEIS. This Letter presents the scattering condition in which the effect of SOC becomes remarkable. The surface analyses using low-energy electron-spin-polarized beams should be carefully made in such a condition.

We performed experiments in an ultrahigh vacuum chamber (base pressure of $5 \times 10{-}11$ Torr) equipped for SP-ISS. Electron-spin-polarized $^4He^+$ ions were generated by Penning ionization of spin-polarized He^* [23,24]. We employed an optical pumping technique to spin polarize He^*. The spin polarization of the He^+ ion beam P_{He^+} was

about 0.2 [25]. The spin direction of the incident He^+ ion beam was defined by the guiding field (~ 0.3 Oe), which was perpendicular to both the scattering plane and the surface normal of the target as shown in Fig. 1.

In this study, we performed experiments for 13 samples, each consisting of a form of the pure elements Si, Cu, Zn, Ag, Sn, Hf, Ta, Re, Ir, Pt, Au, Pb, and Bi. We cleaned the sample surface by repeated cycles of annealing and sputtering in ultrahigh vacuum; preliminary ISS measurements confirmed that the cleaning was successful.

Figure 1 shows the ISS spectra and spin asymmetry of gold surfaces. The ISS intensity I and the spin asymmetry A are defined as $I_\uparrow + I_\downarrow$ and $(I_\uparrow - I_\downarrow)/P_{He^+}I$, where $I_\uparrow$ and $I_\downarrow$ are the scattered intensities of projectile ions whose magnetic moments are parallel and antiparallel to the guiding magnetic field $\mathbf{B}$, respectively. In the ISS spectrum, the scattering peak of gold is observed at 1410 eV in addition to the secondary ions below 100 eV. The position of the gold peak is consistent with the He^+-Au binary collision energy. Because gold is a nonmagnetic material, the neutralization probability of the incident He^+ ions with up spins should be equal to that with down spins. Therefore, the gold surface is not expected to exhibit spin asymmetry. However, it is clearly observed at the elastic peak position of gold; it becomes maximum at the He^+-Au binary collision energy. Considering that the spin asymmetry of the Fe(100) surface in the magnetic remanent state is about 5% [6], this spin asymmetry (about 9%) is obviously not due to the diamagnetism of gold because the magnetic susceptibility of gold (-3×10^{-11} $m^3 \cdot mol^{-1}$ [26]) is too small to explain it. The absence of spin asymmetry of secondary ions reveals that the spin asymmetry at the gold peak is not due to fluctuations in the incident ion beam current. Actually, we confirmed that the fluctuation in the beam current is much less than 1% from direct analysis by a picoammeter placed between the electrically floated target and ground. The agreement of the spin asymmetry in single crystalline and polycrystalline gold in Fig. 1 indicates that the target crystal structure has no effect; in other words, the fact that the target is solid has no effect. These considerations indicate that the spin asymmetry arises from the He^+-Au binary collision. This is proven by the experimental observation that the spin asymmetry of gold was independent of both the incident and the exit angles (not shown), i.e., the projectile trajectory near the surface. The neutralization of the projectile ion is sensitive to its trajectory because of neighboring atoms of the collision partners [27], so these results indicate that ion neutralization has no effect on the spin asymmetry on nonmagnetic surfaces. Thus, it should be attributed to the scattering cross section.

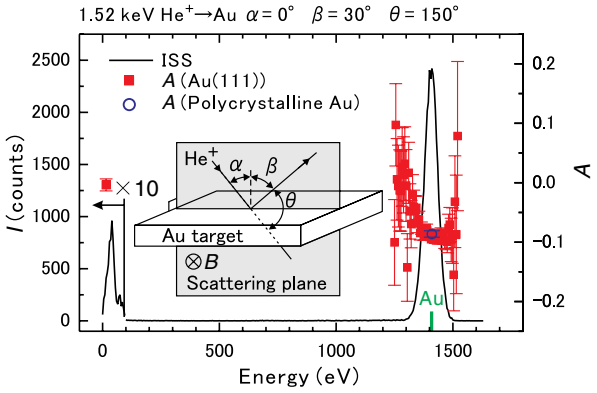

FIG. 1 (color online). ISS spectrum (black curve) of the Au(111) surface with the calculated He^+-Au binary collision energy (green bar). Filled red squares represent the spin asymmetries of Au(111); an open blue circle indicates that of polycrystalline Au. The error of the spin asymmetry corresponds to statistics. The inset shows the scattering geometry. The scattering plane is perpendicular to both the Au surface and the magnetic field $\mathbf{B}$.

The effect of SOC on the scattering cross section has been widely observed with nuclear-spin-polarized light ions such as protons at MeV energies [20–22]. SOC is expected to be larger for electron spins than for nuclear spins because the Bohr magneton is larger than the nuclear magneton by 3 orders of magnitude. Nevertheless, no study has reported the effect of SOC on electron-spin-polarized ion scattering. This may be due to the lack of scattering experiments with well-defined electron-spin-polarized ion beams. The abovementioned results are explained well by SOC as follows.

Here, we discuss the SOC potential U_{SOC} in He^+ ion scattering. For simplicity, we only consider the SOC of the $He^+ 1s$ electron at the smallest He^+-target distance, i.e., the classical turning point. Thus, the effect of SOC arises from the transient angular motion of the $He^+ 1s$ electron around the target nucleus with velocity v_a and radius r_a. Because the center of the $He^+ 1s$ electron distribution coincides with the He^+ nucleus, we assume that the averaged v_a and r_a at the classical turning point are equal to the He^+ nucleus velocity v_{min} and the He^+ ion-target internuclear distance r_{min}, respectively. For Coulomb scattering, we write r_{min} without coefficients as follows [28]:

$$r_{min} \propto \frac{Z_2}{v_0^2}\left[1 + \frac{1}{\sin(\theta/2)}\right], \tag{2}$$

where v_0 denotes the incident velocity of the projectile. Since the targets are much heavier than the projectile, we use the same scattering angles for the laboratory and center-of-mass reference frames in Eq. (2). We write v_{min} as

$$v_{min} = 2v_0 \cos(\theta/2). \tag{3}$$

In our experimental setup, the angular momentum $\mathbf{L}(= \mathbf{r}_{min} \times M_1 \mathbf{v}_{min})$ is parallel or antiparallel to $\mathbf{S}$ (see the inset of Fig. 1). Thus, the SOC potential $U_{SOC}^{r_{min}}$ at the smallest He^+-target distance is written as

$$U_{\mathrm{SOC}}^{r_{\mathrm{min}}} \propto \pm \frac{Z_2 v_{\mathrm{min}}}{r_{\mathrm{min}}^2}. \quad (4)$$

The sign of $U_{\mathrm{SOC}}^{r_{\mathrm{min}}}$ depends on the He^+ ion spins. From Eqs. (2)–(4), we know that SOC disappears at $\theta = 0°$ and 180°, whereas it has a single maximum between these angles. We can intuitively understand this θ dependence by considering the relationship between SOC and the impact parameters. Accordingly, we infer a sinusoidal-like relationship for the A-θ curve, and this is confirmed as follows.

Because U_{SOC} is much smaller than the central force potential U_C in our experiment, we approximate the total scattering potential U as follows:

$$U = U_C + U_{\mathrm{SOC}} \sim \frac{U_C^{r_{\mathrm{min}}} + U_{\mathrm{SOC}}^{r_{\mathrm{min}}}}{U_C^{r_{\mathrm{min}}}} U_C = (1 \pm K) U c, \quad (5)$$

where $K \propto v_{\mathrm{min}}/r_{\mathrm{min}}$. In Eq. (5), the coefficient of the central force potential represents the effect of SOC. Therefore, we obtain the expression for the spin asymmetry A using the conventional derivation for the scattering cross section in Rutherford scattering [29]:

$$A = \frac{(1+K)^2 - (1-K)^2}{(1+K)^2 + (1-K)^2} \propto \frac{v_0^3 \cos(\theta/2)}{Z[1 + \frac{1}{\sin(\theta/2)}]}. \quad (6)$$

The approximation $1 \pm K \sim 1$ is used to derive Eq. (6). Note that the signs of the spin asymmetry for scattering to the left and right should be opposite as seen from the incident beams (θ and θ', respectively, in Fig. 2). The theoretical A-θ curve agrees with the typical experimental result in Fig. 2, which was obtained on a polycrystalline lead surface.

In Eq. (1), U_{SOC} is proportional to $\mathbf{L} \cdot \mathbf{S}$; therefore, the spin asymmetry becomes maximum (zero) when the guiding field is perpendicular (parallel) to the scattering plane. We experimentally observed this relationship by changing the guiding field using the three-axis coil surrounding the entire apparatus. From these results, we conclude that the spin asymmetry on nonmagnetic surfaces is due to SOC acting transiently on the He^+ ion spins in the binary collisions. Thus, the spin asymmetry should also appear in gas-phase collisions, although, to the best of our knowledge, no study has reported such effects in gas-phase collisions.

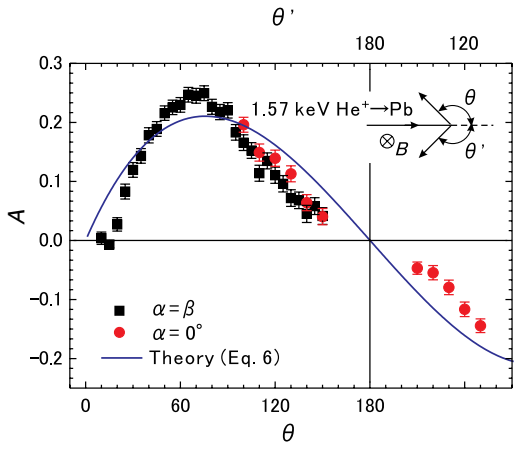

FIG. 2 (color online). Spin asymmetry of Pb as a function of scattering angles θ and θ' for $\alpha = \beta$ (black squares) and $\alpha = 0°$ (red circles). The inset shows the definitions of θ and θ', which correspond to scattering to the left and right, respectively, as seen from the projectile.

The spin-dependent He^+ ion scattering in the present study resembles Mott scattering in the sense that the radial force for electrons in the collision induced by SOC is the origin of the spin-dependent scattering cross section. The spin dependence in Mott scattering is characterized by the Sherman function $S(\theta)$ as $\sigma(\theta) \propto 1 + S(\theta)\mathbf{P} \cdot \hat{\mathbf{n}}$, where $\mathbf{P}$ and $\hat{\mathbf{n}}$ are the polarization vector and the unit vector perpendicular to the scattering plane, respectively [30]. Thus, A in Fig. 2 corresponds to the Sherman function in Mott scattering. Note that the velocity of He^+ ions is much smaller than that of electrons with the same collisional energy. The strong coupling between the nucleus and the electron in He^+ ions enables the close approach of the $He^+ 1s$ electron to the target by the nuclear motion of He^+ ions.

According to Eq. (6), the spin asymmetry should be proportional to the third power of v_0. We generally observed a monotonic increase in the spin asymmetry with v_0. A typical result obtained for the Au(111) surface is shown in Fig. 3; it is consistent with our interpretation. The amplitude of the oscillatory structure in the A-θ curve shown in Fig. 2 increases with v_0 because of the v_0 dependence of SOC. However, we observed that a change in v_0 does not affect the shape of the A-θ curve. Thus, the scattering angle for the maximal spin asymmetry is not related to v_0. This is also consistent with Eq. (6).

We observed no spin asymmetry at $E_0 < 500$ eV on any target. For example, in Fig. 3, the asymmetry on gold almost disappears at $v_0 = 1.5 \times 10^5$ m/s (~ 470 eV). Thus, this result supports the traditional assumption of a

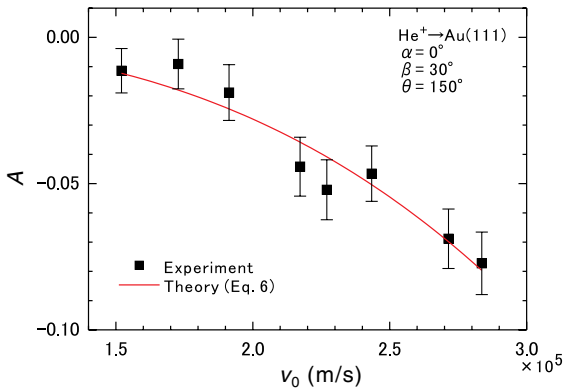

FIG. 3 (color online). Spin asymmetry of Au as a function of the incident velocity with the theoretical curve from Eq. (6).

spin-independent scattering cross section with a thermal collisional energy in SP-MDS.

It is physically probable that the increase in the spin asymmetry with v_0 has an upper limit somewhere below 100%, which does not appear in Eq. (6). The mechanism should involve SOC, which also acts as the origin of the spin flip. In strong SOC, **S** is not conserved, but the total angular momentum $\mathbf{J} = \mathbf{L} + \mathbf{S}$ is maintained; that is, J and m_J are good quantum numbers. Thus, the mixing nature of spins in SOC, i.e., spin relaxation, enhanced with v_0 prevents the spin asymmetry from approaching 100% [31–34]. A higher spin relaxation rate, that is, stronger SOC, is expected with smaller $r_{\min}$, i.e., a lighter target [Eq. (2)]. We observed no spin asymmetry on light element targets such as Si, Cu, and Zn. On the other hand, heavy element targets such as Pb and Bi exhibited a large spin asymmetry.

The spin asymmetry roughly increases with the atomic mass of the target, as previously mentioned. This target element dependence is similar to Mott scattering for electrons [30]. However, the detailed target element dependence is complex because it is determined from both SOC and reionization. For example, we observed that the spin asymmetry of Ag is much larger than that of Hf although Hf is heavier than Ag. Next, we briefly discuss the role of reionization in the target element dependence.

Reionization is the ionization process of He^0, which originates in the neutralization of the He^+ ion on its incoming trajectory. The reionization mechanism is electron promotion mediated by a collisional quasimolecule [35]. Because reionization is spin independent, the number of He^+ ions originating in reionization should be equally divided between up and down spins. Thus, the effective He^+ ion beam polarization P'_{He^+} after reionization is written as follows:

$$P'_{He^+} = P_{He^+} \frac{1 - P_N}{1 - P_N + P_R P_N}, \tag{7}$$

where $P_N (= 1 - P_S)$ and P_R denote the probabilities of neutralization and reionization, respectively. Equation (7) shows that the spin asymmetry is affected by the factor $P'_{He^+}/P_{He}[= (1 - P_N)/(1 - P_N + P_R P_N)]$ if reionized He^+ ions are involved in the appearance of the spin asymmetry. In other words, if the spin asymmetry arises from the collision process, it should follow P'_{He^+}/P_{He^+}. We observed this relationship in Fig. 4 with the fitting parameter of P_N. A comparison with the previously reported P_R value yields $P_N = 0.91$ [35], which is consistent with past reports [4]. The agreement between the spin asymmetry and the effective He^+ ion beam polarization is consistent with our interpretation of SOC in ion scattering.

The inset in Fig. 4 compares a clean platinum surface with a platinum surface after an O_2 exposure of 6 L ($= 10^{-6}$ Torr · s) at 293 K. In accordance with previous studies [36], the exposed platinum surface is covered with oxygen as observed by ISS, in which the spectra are normalized to the incident beam current. The significant increase in the Pt peak confirms the change in the electronic state around the platinum atom owing to the O_2 exposure. Thus, the ion neutralization probability should be greatly modified by oxygen adsorption [37]. However, the spin asymmetries of these two platinum surfaces are equivalent. We also observed that further exposure to O_2 up to 100 L caused no significant change in the spin asymmetry. Moreover, we generally observed that surface contamination had no effect on the asymmetry not only on platinum surfaces but also on other nonmagnetic surfaces. These results are consistent with our interpretation of the spin-dependent scattering cross section.

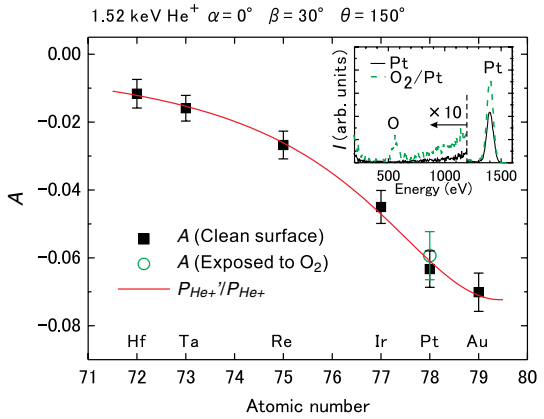

FIG. 4 (color online). Spin asymmetries for 5*d* transition metals with the theoretical curve obtained from the effective beam spin polarization (P'_{He^+}/P_{He^+}) after reionization. The inset shows the ISS spectra of clean (solid black curve) and oxygen adsorbed (dotted green curve) Pt surfaces.

Finally, we comment on the application of SOC in electron-spin-polarized ion sources. The present study demonstrates that the scattering cross section depends on the He^+ ion spin on nonmagnetic surfaces. This clearly indicates that He^+ ions are generally polarized after scattering. Thus, nonmagnetic surfaces act as a polarizer. Because SOC polarizes the projectile if it has an electron spin, such a polarizer is probably applicable to atomic species other than He^+ ions. Previous studies have already realized such electron-spin-polarization techniques in electron-atom scattering [30]. However, no study has demonstrated electron spin polarization in atom-atom or ion-atom collisions. If the polarizer is feasible for generating polarized ion beams, we would not need optical pumping, which often requires an expensive laser.

The applicability of such a polarizer depends on the scattered ion yield. A heavy element target is appropriate for the polarizer in terms of both the beam polarization and the scattering cross section. For a lead target, the counting rate was a few thousand counts per second with the analyzer at an acceptance angle of 5°, a working distance of

25 mm, and a scattering angle of 70°. From the current density of the incident beam (~ 0.1 nA $\cdot$ mm^{-2}), we estimated the decrease in the current density after scattering as being roughly 5 orders of magnitude. Thus, the polarized $^4He^+$ ion beam with P_{He^+} of 25% (Fig. 2) and a density of 0.1 nA $\cdot$ mm^{-2} may be available with this scattering geometry using a primary beam with a density of 10 μA $\cdot$ mm^{-2}. This current density is feasible if an intense ion source such as a duoplasmatron type is used [38].

The authors thank Professor X. M. Tong, Professor N. Toshima, Dr. R. Souda, Professor H. Winter, Dr. M. Kurahashi, Dr. M. Kato, Professor K. Kimura, Professor M. Tanaka, and Professor Y. Yamazaki for useful discussions. This work was partially supported by SENTAN-JST and KAKENHI No. 22760032.

*Corresponding author.
suzuki.taku@nims.go.jp

[1] H. H. Brongersma, M. Draxler, M. de Ridder, and P. Bauer, Surf. Sci. Rep. **62**, 63 (2007).
[2] B. W. Ward, J. A. Notte, and N. P. Economou, J. Vac. Sci. Technol. B **24**, 2871 (2006).
[3] Yu. Bandurin, V. A. Esaulov, L. Guillemot, and R. C. Monreal, Phys. Rev. Lett. **92**, 017601 (2004).
[4] M. Draxler, R. Gruber, H. H. Brongersma, and P. Bauer, Phys. Rev. Lett. **89**, 263201 (2002).
[5] D. L. Bixler, J. C. Lancaster, F. J. Kontur, P. Nordlander, G. K. Walters, and F. B. Dunning, Phys. Rev. B **60**, 9082 (1999).
[6] T. Suzuki and Y. Yamauchi, Surf. Sci. **602**, 579 (2008).
[7] H. Winter, Phys. Rep. **367**, 387 (2002).
[8] T. T. Suzuki, H. Kuwahara, and Y. Yamauchi, Surf. Sci. **604**, 1767 (2010).
[9] M. Onellion, M. W. Hart, F. B. Dunning, and G. K. Walters, Phys. Rev. Lett. **52**, 380 (1984).
[10] C. S. Arnold and D. P. Pappas, Phys. Rev. Lett. **85**, 5202 (2000).
[11] M. Kurahashi, T. Suzuki, X. Ju, and Y. Yamauchi, Jpn. J. Appl. Phys. **42**, 4698 (2003).
[12] M. Bode, M. Heide, K. von Bergmann, P. Ferriani, S. Heinze, G. Bihlmayer, A. Kubetzka, O. Pietzsch, S. Blugel, and R. Wiesendanger, Nature (London) **447**, 190 (2007).
[13] M. Gruyters, T. Bernhard, and H. Winter, Phys. Rev. Lett. **94**, 227205 (2005).
[14] C. L. Gao, U. Schlickum, W. Wulfhekel, and J. Kirschner, Phys. Rev. Lett. **98**, 107203 (2007).
[15] T. T. Suzuki, H. Sukegawa, and K. Inomata, Phys. Rev. B **79**, 045423 (2009).
[16] M. Kurahashi, T. Suzuki, X. Ju, and Y. Yamauchi, Surf. Sci. **552**, 193 (2004).
[17] M. Getzlaff, D. Egert, P. Rappolt, M. Wilhelm, H. Steidl, G. Baum, and W. Raith, J. Magn. Magn. Mater. **140-144**, 727 (1995).
[18] P. Ferro, R. Moroni, M. Salvietti, M. Canepa, and L. Mattera, Surf. Sci. **407**, 212 (1998).
[19] S. P. Weppner, R. B. Penney, G. W. Diffendale, and G. Vittorini, Phys. Rev. C **80**, 034608 (2009).
[20] M. Y. M. Hassan, M. Y. H. Farag, E. H. Esmael, and H. M. Maridi, Phys. Rev. C **79**, 014612 (2009).
[21] V. K. Lukyanov, E. V. Zemlyanaya, K. V. Lukyanov, D. N. Kadrev, A. N. Antonov, M. K. Gaidarov, and S. E. Massen, Phys. Rev. C **80**, 024609 (2009).
[22] X. Li, H. An, and C. Cai, Eur. Phys. J. A **39**, 255 (2009).
[23] T. Suzuki and Y. Yamauchi, Nucl. Instrum. Methods Phys. Res., Sect. A **575**, 343 (2007).
[24] D. L. Bixler, J. C. Lancaster, F. J. Kontur, R. A. Popple, and F. B. Dunning, Rev. Sci. Instrum. **70**, 240 (1999).
[25] T. Suzuki and Y. Yamauchi, Phys. Rev. A **77**, 022902 (2008).
[26] D. R. Lide, *CRC Handbook of Chemistry and Physics* (CRC Press, Boca Raton, 2008).
[27] L. Houssiau, J. W. Rabalais, J. Wolfgang, and P. Nordlander, Phys. Rev. Lett. **81**, 5153 (1998).
[28] M. Nastasi, J. W. Mayer, and J. K. Hirvonen, *Ion-Solid Interactions* (Cambridge University Press, Cambridge, England, 1996).
[29] A. Messiah, *Quantum Mechanics* (North-Holland, Amsterdam, 1962), Vol. 2.
[30] J. Kessler, *Polarized Electrons* (Springer-Verlag, Berlin, 1976).
[31] W. Happer, Y. Y. Jau, and T. G. Walker, *Optically Pumped Atoms* (Wiley-VCH, Weinheim, 2010).
[32] M. A. Bouchiat, J. Brossel, and L. C. Pottier, J. Chem. Phys. **56**, 3703 (1972).
[33] S. E. Maxwell, M. T. Hummon, Y. Wang, A. A. Buchachenko, R. V. Krems, and J. M. Doyle, Phys. Rev. A **78**, 042706 (2008).
[34] D. K. Walter, W. M. Griffith, and W. Happer, Phys. Rev. Lett. **88**, 093004 (2002).
[35] R. Souda, T. Aizawa, C. Oshima, S. Otani, and Y. Ishizawa, Phys. Rev. B **40**, 4119 (1989).
[36] S. Helveg, H. T. Lorensen, S. Horch, E. Lgsgaard, I. Stensgaard, K. W. Jacobsen, J. K. Nrskov, and F. Besenbacher, Surf. Sci. **430**, L533 (1999).
[37] R. Souda, Int. J. Mod. Phys. B **14**, 1139 (2000).
[38] I. G. Brown, *The Physics and Technology of Ion Sources* (Wiley-VCH, Weinheim, 2004).